8-28-2016

Direct Bandgap Cross-over Point of $Ge_{1-y}Sn_y$ Grown on Si Estimated through Temperature-dependent Photoluminescence Studies

Thomas R. Harris
Air Force Institute of Technology

Mee-Yi Ryu
Kangwon National University

Yung Kee Yeo
Air Force Institute of Technology

Buguo Wang
Air Force Institute of Technology

C. L. Senaratne
Arizona State University

Recommended Citation

Thomas R. Harris, Mee-Yi Ryu, Yung Kee Yeo, Buguo Wang, C. L. Senaratne, John Kouvetakis; Direct bandgap cross-over point of Ge1-ySny grown on Si estimated through temperature-dependent photoluminescence studies. Journal of Applied Physics 28 August 2016; 120 (8): 085706. https://doi.org/10.1063/1.4961464

Journal of Applied Physics

RESEARCH ARTICLE | AUGUST 29 2016

Direct bandgap cross-over point of $Ge_{1-y}Sn_y$ grown on Si estimated through temperature-dependent photoluminescence studies

Thomas R. Harris; Mee-Yi Ryu; Yung Kee Yeo; Buguo Wang; C. L. Senaratne; John Kouvetakis

Journal of Applied Physics 120, 085706 (2016)
https://doi.org/10.1063/1.4961464

Direct bandgap cross-over point of $Ge_{1-y}Sn_y$ grown on Si estimated through temperature-dependent photoluminescence studies

Thomas R. Harris,[1,a)] Mee-Yi Ryu,[2,b)] Yung Kee Yeo,[1] Buguo Wang,[1] C. L. Senaratne,[3] and John Kouvetakis[3]
[1]*Department of Engineering Physics, Air Force Institute of Technology, Wright-Patterson AFB, Ohio 45433, USA*
[2]*Department of Physics, Kangwon National University, Chuncheon 200-701, South Korea*
[3]*School of Molecular Science, Arizona State University, Tempe, Arizona 85287, USA*

(Received 19 May 2016; accepted 9 August 2016; published online 29 August 2016)

Epitaxial $Ge_{1-y}Sn_y$ ($y = 0\%–7.5\%$) alloys grown on either Si or Ge-buffered Si substrates by chemical vapor deposition were studied as a function of Sn content using temperature-dependent photoluminescence (PL). PL emission peaks from both the direct bandgap (Γ-valley) and the indirect bandgap (L-valley) to the valence band (denoted by E_D and E_{ID}, respectively) were clearly observed at 125 and 175 K for most $Ge_{1-y}Sn_y$ samples studied. At 300 K, however, all of the samples exhibited dominant E_D emission with either very weak or no measureable E_{ID} emission. At 10 K, E_D is dominant only for $Ge_{1-y}Sn_y$ with $y > 0.052$. From the PL spectra taken at 125 and 175 K, the unstrained indirect and direct bandgap energies were calculated and are plotted as a function of Sn concentration, the results of which show that the indirect-to-direct bandgap transition occurs at ∼6.7% Sn. It is believed that the true indirect-to-direct bandgap cross-over of unstrained $Ge_{1-y}Sn_y$ might also take place at about the same Sn content at room temperature. This observation suggests that these $Ge_{1-y}Sn_y$ alloys could become very promising direct bandgap semiconductor materials, which will be very useful for the development of various new novel Si- and Ge-based infrared optoelectronic devices that can be fully integrated with current technology on a single Si chip. *Published by AIP Publishing*. [http://dx.doi.org/10.1063/1.4961464]

I. INTRODUCTION

Silicon has been the amazing material for electronic devices and integrated circuit applications for decades. However, despite the successful demonstration of many Si-compatible photonic devices such as photodiodes,[1] modulators,[2] and waveguides,[3] efficient light sources based on Si or Ge are still very limited, mainly due to the indirect bandgap nature of these materials. Because of this, there has been significant interest in developing Si- and Ge-based direct bandgap semiconductors to expand the functionalities of these materials well beyond electronics. It has been predicted[4–8] that direct bandgap $Ge_{1-y}Sn_y$ alloys could be achieved by incorporating about 6.5%–10% Sn into Ge. Sn reduces the direct bandgap at the Γ-point faster than the indirect bandgap at the L-point and thus reduces the so called Γ–L separation, which is only 140 meV for pure Ge. Therefore, the $Ge_{1-y}Sn_y$ alloy system was extensively pursued as a good candidate for direct bandgap semiconductor materials and as an alternative to direct bandgap Ge-on-Si, which requires high levels of tensile strain (∼2%), and/or heavy n-type doping to overcome the energy difference between the direct and indirect bandgaps.

Toward this end, an intensive research effort was made in recent years to grow device quality epitaxial $Ge_{1-y}Sn_y$ films. As a result, significant breakthroughs have been made not only in the growth of direct bandgap $Ge_{1-y}Sn_y$ alloys with high Sn contents, but also in the development of photonic devices based on these materials. For example, $Ge_{1-y}Sn_y$-based optoelectronic devices such as modulators, photodetectors, light-emitting diodes, and optically pumped laser diodes have already been successfully developed, showing great potential for Si photonic applications.[9–13] Specifically, Wirths *et al.*[8] demonstrated lasing from a direct-bandgap $Ge_{0.874}Sn_{0.126}$ alloy grown on Ge-buffered Si at low temperatures under relatively high levels of optical pumping. In spite of the tremendous recent progress in crystal growth and device fabrication, several important issues still remain, such as good thick, device-quality direct bandgap GeSn alloys, the development of mature doping technology able to achieve the high levels needed for electrically injected laser diodes, the demonstration of a GeSn laser operating in continuous-wave mode at room temperature (RT), the development of a complementary metal-oxide-semiconductor (CMOS) compatible optical amplifier, and a new Ge or GeSn-on-Si wave guiding platform.[14]

Along with the successful crystal growth of device quality epitaxial $Ge_{1-y}Sn_y$ layers, the unique optical properties of these alloys have been characterized. Several groups[7,8,15–18] have performed temperature- (T-) and excitation-laser power-dependent photoluminescence (PL) and photoreflectance measurements of $Ge_{1-y}Sn_y$ samples in order to better understand the indirect- and/or direct-bandgap nature of these alloys and to attempt to better determine at what Sn concentration the indirect-to-direct bandgap cross-over occurs. It has been reported[5,6,8,19] that the transition from indirect to direct

[a)]Present address: Sensors Directorate, Wright Patterson AFB, Ohio 45433, USA.
[b)]Author to whom correspondence should be addressed. Electronic mail: myryu@kangwon.ac.kr. Tel.: +82 33 250 8474. Fax: +82 33 259 5666.

bandgap occurred for fully relaxed GeSn alloys with Sn contents of ~6%–9% using RT or T-dependent PL measurements. Nevertheless, it is still uncertain where the exact crossover point in $Ge_{1-y}Sn_y$ alloys lies. This is due in part to the fact that the direct bandgap (E_D) and indirect bandgap (E_{ID}) PL peaks usually cannot be observed simultaneously at all samples with different Sn compositions and at all temperatures. For example, typically E_{ID} PL peak is dominant at lower temperatures whereas E_D PL peak is dominant at higher temperatures (up to and including RT). Therefore, it is hard to directly observe or claim that E_D PL peak occurs at lower energy than E_{ID} PL peak, which confirms a direct bandgap behavior of the material. In this paper, the results of a systematic temperature-dependent PL study of $Ge_{1-y}Sn_y$ alloys with Sn compositions from 0% to 7.5% are reported. The PL data show both E_D and E_{ID} PL peaks in the same spectrum for almost all $Ge_{1-y}Sn_y$ alloys at temperatures of 125 and 175 K, leading to strong evidence of the true indirect-to-direct bandgap transition at an Sn composition of about 6.7%.

II. EXPERIMENTAL DETAILS

$Ge_{1-y}Sn_y$ films were grown either on Ge-buffered Si substrates ($y = 1.7\%–7.5\%$) or directly on Si substrates ($y = 0.0\%–0.03\%$) using an ultra-high vacuum chemical vapor deposition method. Some $Ge_{1-y}Sn_y$ samples with lower Sn composition (<6%) were deposited by using digermane (Ge_2H_6) and stannane (SnD_4) as precursors while other samples with higher-Sn concentrations used trigermane (Ge_3H_8) for the Ge-source. Table I shows the Sn composition, annealing conditions, residual strain, and thicknesses of $Ge_{1-y}Sn_y$ and Ge layers used in this study. More detailed information on the growth of these materials as well as the characterization methods used to determine Sn concentration, strain state, and layer thickness can be found in Refs. 6 and 20. The strain in the as-grown $Ge_{1-y}Sn_y$ ($y = 0.0\%–0.03\%$) epitaxial layers grown on Si substrates was initially slightly compressive. However, the strain became fully relaxed after annealing at temperatures of 825–830 °C for 30 min, and then changed to slightly tensile upon cooling to RT due to the large difference in thermal expansion coefficients between $Ge_{1-y}Sn_y$ and Si. The final residual strain value for both Ge and $Ge_{0.9997}Sn_{0.0003}$ was 0.19% according to high resolution X-ray diffraction measurements. The residual strain in the as-grown $Ge_{1-y}Sn_y$ ($y > 1.7\%$) layers grown on Ge-buffered Si was compressive while the strain for the 1.7% Sn sample which underwent three cycles of rapid thermal annealing (RTA) at 650 °C for 2 s was tensile due to the thermal expansion mismatch mentioned previously. However, it is worth noting that the strain for $Ge_{0.925}Sn_{0.075}$ sample is still slightly compressive even after three cycles of RTA at a temperature of 550 °C for 2 s as shown in Table I. T-dependent PL measurements were carried out at temperatures ranging from 10 to 300 K. The samples were excited by 830 nm radiation from a tunable Ti-Sapphire laser pumped by an Ar-ion laser. The laser beam was focused to a spot size of around 200 μm with laser power ranging from 150–830 mW. The luminescence was dispersed by a $^1/_2$-m spectrometer with either a 1.6 or 2.0 μm blazed grating and collected by either a thermoelectric (TE) cooled, or liquid nitrogen (LN_2) cooled extended InGaAs detector. The TE cooled extended InGaAs detector (cut-off at 2.05 μm) was used for samples with $Sn \leq 4.3\%$, while the LN_2 cooled extended InGaAs detector (cut-off at 2.3 μm) was used for samples with $Sn \geq 5.2\%$. The $Ge_{1-y}Sn_y$ films were unintentionally doped and all showed n-type conductivity at 300 K with the exception of the $Ge_{0.925}Sn_{0.075}$ film, which showed p-type conductivity.

TABLE I. Summary of various information on $Ge_{1-y}Sn_y$ samples used in this study.

Sn(%)	Anneal	Strain at RT(%)	Thickness of $Ge_{1-y}Sn_y$ (nm)	Thickness of Ge buffer (nm)
0.0	830 °C/30 min	−0.19	680 (Ge)	…
0.03	825 °C/30 min	−0.19	800	…
1.7	3×(650 °C/2 s)	−0.11	950	1125
3.1	as-grown	+0.06	565	1235
3.7	as-grown	+0.07	650	1500
4.3	as-grown	+0.11	635	540
5.2	as-grown	+0.10	800	850
6.2	as-grown	+0.13	735	775
7.5	3 × (550 °C/2 s)	+0.05	610	440

III. RESULTS AND DISCUSSION

The T-dependent PL spectra of various $Ge_{1-y}Sn_y$ samples ranging from $y = 0\%–7.5\%$ were investigated at temperatures ranging from 10–300 K with a typical laser power of 500 mW. T-dependent PL spectra taken with a laser power of 500 mW of an unintentionally doped $Ge_{0.957}Sn_{0.043}$ sample ($n = 1.6 \times 10^{17}$ cm^{-3}) are shown in Fig. 1(a). This sample had a compressive strain of 0.11% and it clearly shows both direct and indirect bandgap related PL peaks at most temperatures as shown (only for selected temperatures) in the figure. The measured PL spectra are represented by dotted black lines, the individual fitting curves by red and blue lines, and the sum of the fitting curves by green lines. As seen in the figure, the combined fitting curves match the PL spectra very well. The main peak at 0.667 eV, which is very strong at 300 K and becomes a very weak PL peak at 13 K, is assigned to E_D emission while the strong peak centered around 0.676 eV at 13 K, which becomes a very weak PL peak at 300 K, is assigned to E_{ID} related emission. Clearly distinguishable direct and indirect bandgap related emissions can be observed between 13 and 300 K for this sample, which are not readily clearly observable for other samples. The estimated PL peak positions are indicated with red (E_{ID}) and blue arrows (E_D). Apparently, the photo-excitation of electrons out of the valence bands into both Γ and L valleys is efficient at a laser power of 500 mW and a wavelength of 830 nm (1.49 eV). The evolution of the PL intensities of both E_D and E_{ID} can clearly be observed as T changes from low to higher Ts. As seen in the figure, the PL intensity of E_D emission increases gradually as T increases up to RT, which is due in part to the thermalization of electrons from the L-valley to the Γ-valley and also to the relatively efficient direct bandgap transition compared with the phonon-assisted indirect

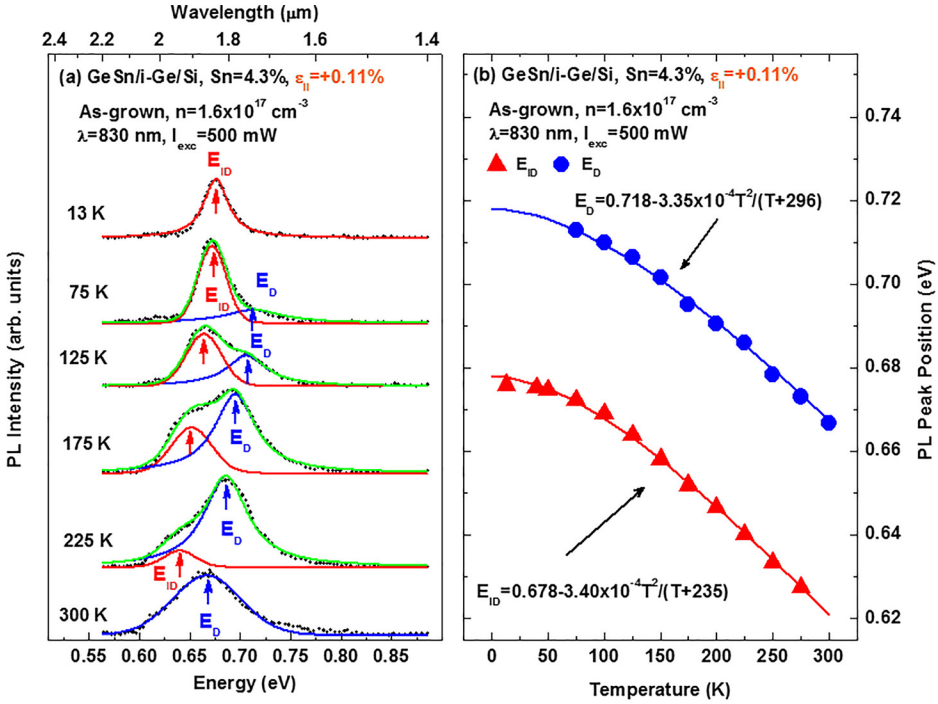

FIG. 1. (a) Selected temperature-dependent PL spectra of compressively strained (+0.11%), unintentionally doped n-$Ge_{0.957}Sn_{0.043}$ grown on Ge-buffered Si substrate taken with a laser power of 500 mW. The observed PL spectra are drawn in dotted black line, the individual fitting curves are shown in red and blue lines for indirect and direct bandgap transitions, respectively, and the sum of the fitting curves are in green line. The best estimated direct bandgap emission peak E_D (blue) and indirect bandgap emission peak E_{ID} (red) are indicated with arrows. (b) E_D (blue dots) and E_{ID} (red triangles) PL peak energies plotted as a function of temperature from 13 to 300 K and fitted with a Varshni type equation.

bandgap transition, leading to strong E_D emission at higher Ts. The slightly compressive (+0.11% at RT) sample shows one broad E_D peak at RT, which is most likely the superposition of the heavy-hole (HH) and light-hole (LH) PL peaks ($E_{D,HH}$ and $E_{D,LH}$, respectively). The separation energy between these two peaks for this $Ge_{0.957}Sn_{0.043}$ sample is estimated to be about 9.7 meV at all temperatures between 13 and 300 K because the strain should be independent of temperature due to the negligible thermal expansion mismatch between the GeSn epilayer and the Ge buffer layer. It is, however, believed that E_D PL is mainly due to the transition from the Γ valley to the HH valence band because of the higher density of states relative to the LH valence band. This suggestion was directly observed from the T-dependent PL studies for the tensile strained GeSn with 0.03% Sn content.[16] In this reference, the PL intensities for $Ge_{0.9997}Sn_{0.0003}$ due to both LH and HH transitions are reported to be about the same at 10 K, but as T increases, PL transitions to HH valence band become dominant above about 100 K.

This sample also shows one broad E_{ID} emission peak at 13 K. At present, the exact nature of this PL peak cannot be determined and could be no-phonon (NP) related, acoustic or optical phonon emission related peak. Also, it is not clear whether the E_{ID} PL emission is HH or LH related. However, it is believed that the observed E_{ID} PL at 13 K is mainly due to the transition from the L valley to the upshifted HH valence band rather than the downshifted LH valence band and is related to a NP peak.[16] If on the other hand, the E_{ID} peak at 13 K is attributed to a Ge-like transverse acoustic (TA ≈ 7 meV), longitudinal acoustic (LA ≈ 27 meV), or transverse optical (TO ≈ 37 meV) phonon emission related peak,[21] then the actual indirect bandgap energy would be higher, further reducing the energy difference between E_D and E_{ID}.

The detailed T-dependent PL peak positions corresponding to E_D(T) and E_{ID}(T) emission energies were estimated by fitting each set of PL data mainly with Lorentzian and/or Gaussian peaks, and the results are plotted as a function of T in Fig. 1(b). The fits were performed using a nonlinear fit routine which minimized the error between the measured data and the sum of the fitting curves by adjusting the free parameters, namely, the peak position, intensity, and width of each peak. For example, the E_{ID}(T) peak at 13 K and the E_D(T) at 300 K are fitted with Lorentzian and Gaussian peaks, respectively. Similar peak positions were obtained for Gaussian and Lorentzian fits; however, in some cases using Lorentzian peaks resulted in a much better fit to the overall spectra. The PL peak positions of E_D(T) and E_{ID}(T) are well defined at most temperatures, but the position of the E_D(T) PL peak at below about 75 K and that of E_{ID}(T) at RT cannot be determined reliably due to the lack of clear respective PL peaks at these temperatures. An error range of ±2.5 meV was determined by adjusting the peak positions of the fitted curves and examining the change in the residuals. The solid fitting curve for E_D(T) is calculated using a Varshni type equation[22] with $E_D(T) = E_D(0) - \alpha T^2/(T+\beta)$, where $E_D(0) = 0.718$ eV is used for the direct bandgap, and parameters of $\alpha = 3.35 \times 10^{-4}$ eV/K and $\beta = 296$ K were used which are similar to those for bulk Ge.[23] As shown in Fig. 1(b), the calculated values for E_D(T) agree very well with the PL data (solid blue circles).

Accurate analysis of the T-dependent indirect bandgap PL emissions is difficult because of the involvement of various phonon emission/absorption and NP related transitions. Some examples of more detailed analysis of the T-dependent indirect bandgap related emissions for a tensile strained $Ge_{0.9997}Sn_{0.0003}$ sample can be found in Ref. 16. That paper described that TA and TO phonon emission associated with

the LH band is dominant for T less than 50 K, and the dominant transition changes from TO to LA phonon emission (still LH) for temperatures from 50 to 100 K. Then NP associated with upper LH valence band is dominant for $100\,\mathrm{K} < \mathrm{T} \leq 200\,\mathrm{K}$, and finally NP associated with lower HH valence band is dominant at or above 250 K (including RT) for that tensile strained sample. It is believed that the E_{ID} PL transitions occur mainly to the upper LH valence band for tensile strained samples primarily through NP related emissions; however, for compressively strained samples, the transitions may occur mainly to the upper HH valence band. The solid fitting curve for $E_{ID}(T)$ is also calculated using a Varshni type equation with $E_{ID}(T) = E_{ID}(0) - \alpha T^2/(T+\beta)$, where $E_{ID}(0) = 0.678\,\mathrm{eV}$, $\alpha = 3.40 \times 10^{-4}\,\mathrm{eV/K}$, and $\beta = 235\,\mathrm{K}$ are used. This calculated $E_{ID}(T)$ agrees very well with the PL data as shown in Fig. 1(b) except at RT due to the very weak E_{ID} PL peak. It should be noted that the measured indirect bandgap PL peaks fit very well with one smooth fitting curve. If various possible phonon emission or absorption peaks are associated with these PL transitions from TA (~7 meV) to LO (~37 meV) phonons, then one would expect that the effects of phonon involvement would show up as more scattered PL data points throughout all temperature range unless only small phonon energy is involved. Therefore, the absence of more scattered T-dependent PL data points might indicate that the observed PL peaks are mostly no-phonon and/or small phonon (such as TA) related peaks.

In order to better understand the effect of Sn on the T-dependent PL data, another well resolved set of spectra were taken with a laser power of 825 mW for an unintentionally doped $Ge_{0.948}Sn_{0.052}$ sample ($n = 4.3 \times 10^{16}\ \mathrm{cm}^{-3}$), and the results are shown in Fig. 2(a). This sample is slightly compressive by +0.10% and both clear direct and indirect bandgap PL spectra are observed at almost all temperatures as shown in the figure. The symbols, color schemes, and descriptions of PL spectra of this figure are same as Fig. 1(a). For 300 K, the strong main peak at 0.608 eV and the weak PL peak at 0.571 eV are assigned to E_D and E_{ID} emissions, respectively. In addition, this E_D peak is also believed to be mainly due to transitions from the Γ valley to the upper HH valence band as discussed before for the previous sample. Fortunately, for this sample both E_D and E_{ID} PL peaks at 0.677 and 0.652 eV, respectively, were clearly observed at 10 K in contrast to the $Ge_{0.957}Sn_{0.043}$ and other samples. Similar to the 4.3% Sn sample, it is believed that the observed E_{ID} PL peak at 10 K is mainly due to the NP related transition from the L valley to the upper HH valence band. If it is attributed instead to transverse acoustic (TA ≈ 7 meV) phonon emission, then the difference between E_D and E_{ID} would only be 18 meV. Further, this sample would become a direct bandgap material if the observed E_{ID} peak is attributed to LA (≈27 meV) or TO (≈36 meV) phonon emission, because E_D would then be less than E_{ID}.

The detailed T-dependent PL peak positions corresponding to $E_D(T)$ and $E_{ID}(T)$ emission energies were estimated by fitting each set of $E_D(T)$ and $E_{ID}(T)$ PL data mainly with an exponentially modified Gaussian and a Gaussian peak, respectively, and the results are plotted as a function of T in Fig. 2(b). The error range for these fits is ±5.0 meV, which is slightly larger than those for the previous sample due to the increased overlap between $E_D(T)$ and $E_{ID}(T)$. The solid fitting curve for $E_D(T)$ was calculated using $E_D(T) = E_D(0) - \alpha T^2/(T+\beta)$, where $E_D(0) = 0.677\,\mathrm{eV}$, $\alpha = 4.71 \times 10^{-4}\,\mathrm{eV/K}$, and $\beta = 296\,\mathrm{K}$, and similarly $E_{ID}(T)$ was calculated using $E_{ID}(0) = 0.651\,\mathrm{eV}$, $\alpha = 4.76 \times 10^{-4}\,\mathrm{eV/K}$, and $\beta = 235\,\mathrm{K}$. As with the previous sample, the calculated values of $E_D(T)$ and $E_{ID}(T)$ agree very well with the PL data as shown in Fig. 2(b).

In order to more easily observe the indirect-to-direct bandgap cross-over for these $Ge_{1-y}Sn_y$ samples, the PL spectra along with the E_D and E_{ID} fitting curves are plotted in

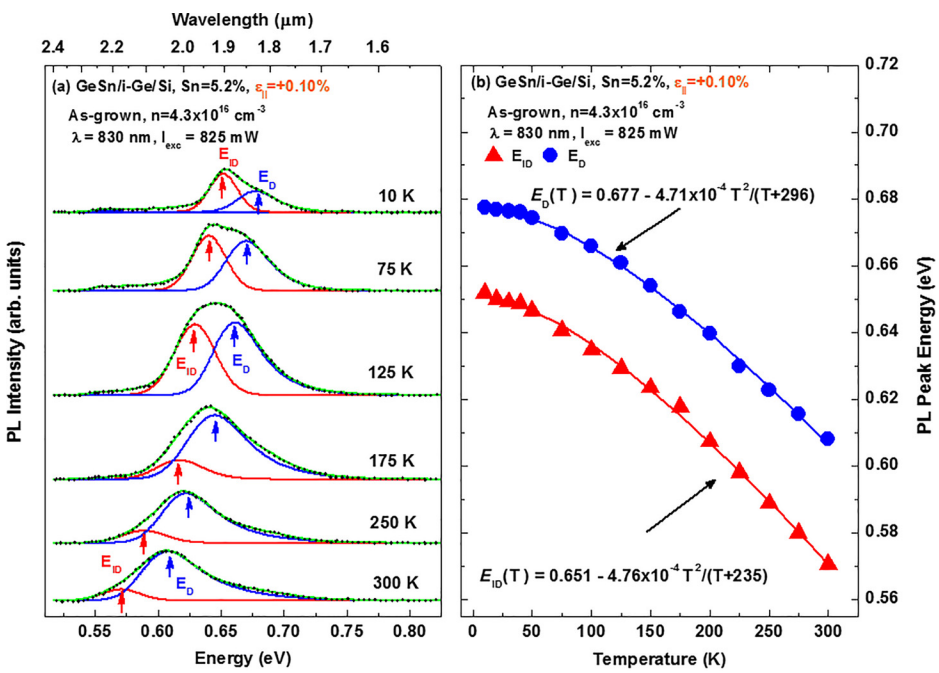

FIG. 2. (a) Selected temperature-dependent PL spectra of compressively strained (+0.10%), intrinsic n-$Ge_{0.948}Sn_{0.052}$ grown on Ge-buffered Si substrate taken with a laser power of 825 mW. The observed PL spectra are drawn in dotted black line, the individual fitting curves are shown in red and blue lines for indirect and direct bandgap transitions, respectively, and the sum of the fitting curves are in green line. The best estimated direct bandgap emission peak E_D (blue) and indirect bandgap emission peak E_{ID} (red) are indicated with arrows. (b) E_D (blue dots) and E_{ID} (red triangles) PL peak energies plotted as a function of temperature from 10 to 300 K and fitted with a Varshni type equation.

Fig. 3(a) for various Sn contents at 175 K. The measured PL spectra are represented by dotted black lines, the E_{ID} and E_D fitting curves by red and blue lines, respectively, and the sum of the fitting curves by green lines. The Sn content and residual strain value for each $Ge_{1-y}Sn_y$ sample is annotated in the figure. As seen in the figure, the combined fitting curves fit the PL spectra very well. A temperature of 175 K instead of room temperature was chosen specifically because all $Ge_{1-y}Sn_y$ samples show both clear direct and indirect bandgap PL peaks at this temperature except for the samples with higher Sn contents (>5.2%). As in previous figures, the estimated PL peak positions are indicated with red (E_{ID}) and blue arrows (E_D). From these data, the true cross-over point can be determined. As shown in Fig. 3(a), the energy difference between E_{ID} and E_D becomes smaller and smaller, with the two peaks merging nearly into one broad peak as Sn content increases up to 7.5%. It is important to note here that the E_{ID} energy is higher than E_D for the 7.5% Sn content sample. Despite the large amount of overlap between the peaks, it is still possible to distinguish E_D from E_{ID} based on the T-dependent relative PL intensities (not shown here). Specifically, for $T > 150$ K, the E_D PL peak intensities must also be much greater than E_{ID} PL peak intensities for the 7.5% Sn content sample just as shown in Figs. 1(a) and 2(a) for the 4.3% and 5.2% Sn content samples, respectively. That is, the dominant PL peak at 175 K for the 7.5% Sn sample must be E_D PL peak as indicated in Fig. 3(a). Furthermore, the E_D peak intensities increase as T decreases even down to 10 K, which is a typical characteristic of direct bandgap semiconductors. Analysis of the full width at half maximum (FWHM) of the E_{ID} and E_D peaks has been performed as a function of Sn content, but it turns out that a detailed analysis of the FWHM was difficult since in general, the FWHM would depend on the strain, phonon involvement for E_{ID} peak, doping level, annealing conditions, and overall quality of each sample. In spite of those facts, as seen in the figure, there is a slight increase in the FWHM of the direct bandgap PL peak as Sn content increases from 1.7% to 6.2%, which could be due in part to alloy broadening as well. However, it can be noticed in the figure that the FWHM for the 7.5% sample is narrower than that of the 6.25% sample. It also showed that the analysis of FWHM (28 meV) at 10 K for the 7.5% sample was much narrower than that (38 meV) of the 6.25% sample, indicating dominant direct bandgap related emission for the 7.5% sample.

In Fig. 3(b), the strain corrected direct bandgap E_D (blue squares) and indirect bandgap E_{ID} (red circles) transition energies are plotted as a function of Sn composition. This figure clearly shows the transition of unstrained $Ge_{1-y}Sn_y$ from an indirect to direct bandgap semiconductor. All of the data points shown in the figure were corrected for residual tensile or compressive strain for each sample, with correction factors calculated using deformation potential theory.[24] The strain correction values for E_D were about 6–15 meV for the compressively strained samples (0.05%–0.13% strain) and 13–40 meV for the tensile strained samples (0.11%–0.26% strain). The strain correction values for E_{ID} are smaller and are about 1.7–4.5 meV and 4–12 meV for the compressive and tensile strained samples, respectively. These strain correction values could be slightly different, depending on the

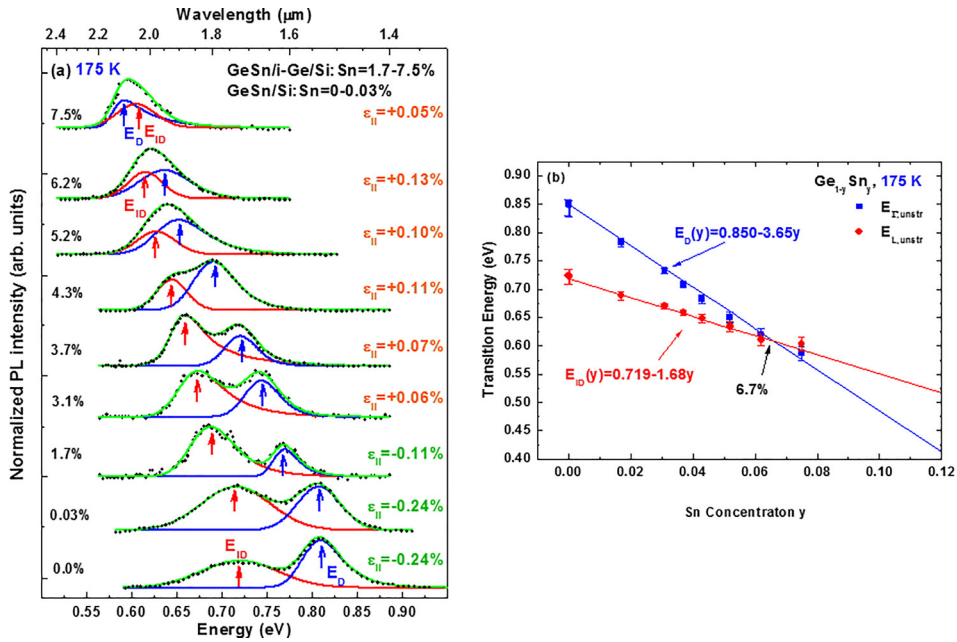

FIG. 3. (a) The PL spectra of epitaxial $Ge_{1-y}Sn_y$ alloys (y = 0%–7.5%) plotted as a function of Sn content taken at a temperature of 175 K. The $Ge_{1-y}Sn_y$ samples for Sn ≤ 1.7% were grown on Si or Ge-buffered Si substrates and have tensile strains (0.11%–0.24%), whereas those for Sn ≥ 3.1% were grown on Ge buffer layers grown on Si substrates and have compressive strains (0.05%–0.13%). The strain value for each sample is indicated in the figure. The observed PL spectra are drawn in dotted black line, the individual fitting curves are shown in red and blue lines for indirect and direct bandgap transitions, respectively, and the sum of the fitting curves are in green line. The best estimated direct bandgap emission peak E_D (blue) and indirect bandgap emission peak E_{ID} (red) are indicated with arrows. (b) E_D (blue squares and curve) and E_{ID} (red dots and curve) PL peak energies at 175 K plotted as a function of Sn concentration. All these PL peak values were strain corrected for relaxed epitaxial $Ge_{1-y}Sn_y$ alloys with error bars. The fitting curves were drawn using linear fits with slopes of 3.65 and 1.68 for E_D and E_{ID}, respectively.

deformation potential used. The tensile strain of the Ge and $Ge_{0.9997}Sn_{0.0003}$ samples grown directly on Si substrates is calculated to increase from 0.19% to 0.26% as temperature decreases from RT to 125 K due to the aforementioned thermal expansion mismatch. The peak positions for the 5.2% Sn sample were upshifted by 10 meV in order to correct for the effects of local laser heating due to the higher laser power of 825 mW used for this sample. As pointed out before, it is very difficult to determine whether the measured E_{ID} PL peak is related to no-phonon, phonon emission, or phonon absorption, or which particular phonon is involved, if any. Therefore, there is some uncertainty in obtaining an accurate bandgap energy E_{ID} from the PL peaks. In Fig. 3(b), it is assumed that the observed E_{ID} PL peaks at 175 K are no-phonon related transitions for these mostly unintentionally doped $Ge_{1-y}Sn_y$ samples. The error bars shown in the figure include only the contributions from the curve fitting error of ± 2.5 to ± 5.0 meV and the uncertainty in the strain correction due to the HH-LH valence band splitting. The possible errors in estimating E_D and E_{ID} arising from phonon absorption or emission as well as any doping effects and superposition of the HH and LH related PL peaks were not considered. For most samples, the error bars are relatively small and for some data points are approximately the same size as the symbols. It is believed that the measured E_D and E_{ID} values are mainly due to transitions from the Γ valley and the L valley to the HH valence band, respectively, for both compressive and tensile strained samples as described above. However, the measured E_{ID} values could also be due to transitions from the L valley to the LH valence band for the tensile strained samples at $T \leq 250$ K.[16] For example, the separation energy between the HH and LH valence bands for the 0.13% compressively strained sample is estimated to be about 11 meV, compared with 17 meV for the 0.19% tensile strained sample. The solid lines in Fig. 3(b) are linear fits with slopes of 3.65 and 1.68 for E_D and E_{ID} transition energies, respectively, which fit the data relatively well for the given range of Sn contents. Based on these fits, the figure shows that the cross-over point of unstrained $Ge_{1-y}Sn_y$ is estimated to be around 6.7% Sn content. Quadratic fits using bowing parameters were also done; however, the results were very similar to the linear fits for the range of Sn contents studied and the predicted crossover value was almost identical. Given the similarities and the wide range of bowing parameter values reported in the literature, it was determined that the linear fits were the best method for evaluating the change in the direct and indirect bandgaps with Sn content. It should be noted that for the 7.5% Sn sample, E_D is lower than E_{ID} and that these two data points are well within the fitting lines given the error bounds.

Another set of well resolved E_D and E_{ID} PL spectra for various $Ge_{1-y}Sn_y$ ($y = 0\%$–7.5%) samples at 125 K are plotted in Fig. 4(a). The symbols, color schemes, and descriptions of the PL spectra for this figure are same as Fig. 3(a). This temperature was chosen because all of the samples show both clear direct and indirect bandgap related PL peaks with slightly better distinguished E_{ID} and E_D PL spectra, especially for 5.2% Sn, compared with 175 K. Also, it should be noted that Fig. 4(a) shows the PL data for strained samples similar to Fig. 3(a). In addition, it should be noted that for the 7.5% Sn sample E_{ID} is again higher than E_D as was the case for 175 K. As mentioned earlier, this was confirmed

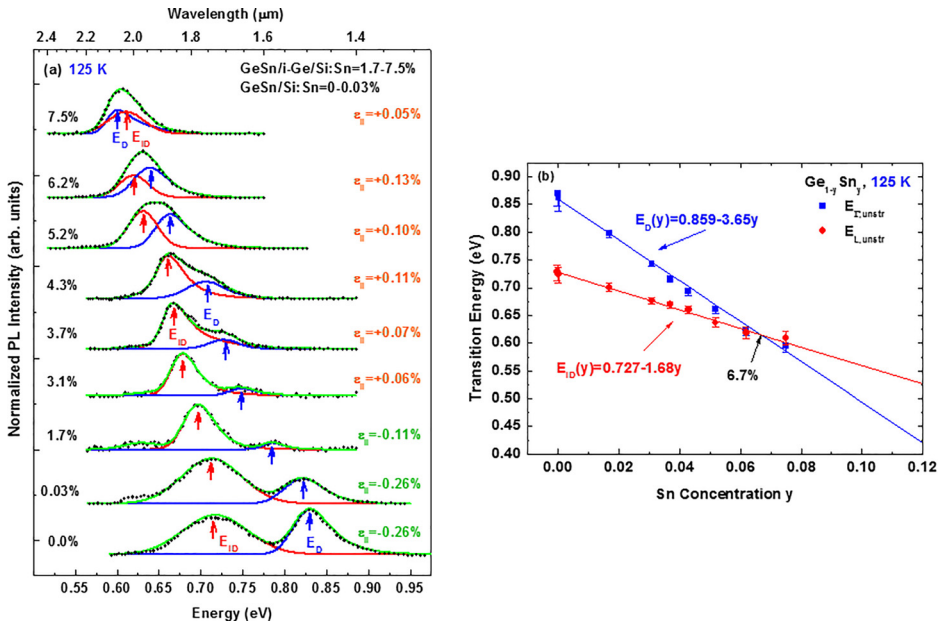

FIG. 4. (a) The PL spectra of epitaxial $Ge_{1-y}Sn_y$ alloys ($y = 0\%$–7.5%) plotted as a function of Sn content taken at a temperature of 125 K. The $Ge_{1-y}Sn_y$ samples for $Sn \leq 1.7\%$ were grown on Si or Ge-buffered Si substrates and have tensile strains (0.11%–0.26%), whereas those for $Sn \geq 3.1\%$ were grown on Ge buffer layers grown on Si substrates and have compressive strains (0.05%–0.13%). The strain value for each sample is indicated in the figure. The observed PL spectra are drawn in dotted black line, the individual fitting curves are shown in red and blue lines for indirect and direct bandgap transitions, respectively, and the sum of the fitting curves are in green line. The best estimated direct bandgap emission peak E_D (blue) and indirect bandgap emission peak E_{ID} (red) are indicated with arrows. (b) E_D (blue squares and curve) and E_{ID} (red dots and curve) PL peak energies at 125 K plotted as a function of Sn concentration. All these PL peak values were strain corrected for relaxed epitaxial $Ge_{1-y}Sn_y$ alloys with error bars. The fitting curves were drawn using linear fits with slopes of 3.65 and 1.68 for E_D and E_{ID}, respectively.

by the T-dependence of the E_D(T) and E_{ID}(T) PL peak positions and intensities for the $Ge_{0.925}Sn_{0.075}$ sample.

As in Fig. 3(b), the unstrained bandgaps E_D (blue squares) and E_{ID} (red circles) are plotted as a function of Sn composition in Fig. 4(b) which include the strain correction for each sample. Here, it was also assumed that the observed E_{ID} PL peaks are no-phonon related transitions as was the case for 175 K. The error bars in the figure are similar to those in Fig. 3(b) for 175 K with the exception of the Ge and $Ge_{0.9997}Sn_{0.0003}$ samples which have some temperature dependent tensile strain. As in Fig. 3(b), the peak positions for the 5.2% Sn sample were upshifted by 10 meV to correct for the effects of laser heating as mentioned previously. The solid lines in Fig. 4(b) are linear fits with slopes of 3.65 and 1.68 for E_D and E_{ID}, respectively. Again, the agreement with the measured data is very good over the given range of Sn contents. The figure also shows that the cross-over point in $Ge_{1-y}Sn_y$ is estimated to be around 6.7% Sn content. As in Fig. 3(b), it should be noted that E_D is lower than the E_{ID} for 7.5% Sn and that these two points are well within the fitting lines.

Finally, Fig. 5(a) shows the PL spectra measured at room temperature for $Ge_{1-y}Sn_y$ (y = 0%–7.5%) samples for comparison with the PL data taken at 125 and 175 K. The E_D PL peaks related to the direct bandgap transitions were clearly observed at room temperature for all of these $Ge_{1-y}Sn_y$ samples. However, the E_{ID} related PL peaks show only very weak PL signals for lower Sn content ($\leq$4.3%) samples as marked with arrows and therefore the exact E_{ID} PL peaks could not be determined well unlike for the cases of 125 and 175 K. Because of this, only best efforts have been made to estimate the E_{ID} and E_D PL peaks, with the corresponding positions marked with arrows for comparison with Figs. 3(a) and 4(a). It is noted that Jiang *et al.*[6] were able to observe the E_{ID} and E_D PL emissions up to y = 5.7% at RT from a series of $Ge_{1-y}Sn_y$ (y = 0%–6%) samples which were produced using similar experimental methods as the samples studied here, using a 980 nm excitation laser which could offer enhanced resolution of the PL peaks at RT. The approximate E_D PL peak positions are plotted as a function of Sn concentration in Fig. 5(b). The data at 300 K show pretty good fitting with $E_D(y) = 0.800–3.65\,y$, which has the same slope with Sn composition as the E_D(y) fitting lines found in Figs. 3(b) and 4(b) for 175 and 125 K, respectively. Here it is noted that the data point of 7.5% Sn is slightly above the fitting line due to close proximity of PL peak position and detector cut-off wavelength at RT. It is also important to realize that when the E_{ID}(T) PL peaks are assumed to be all due mainly to NP related emissions, the difference between direct and indirect bandgaps [$E_D - E_{ID}$] is about 33, 34, and 37 meV for the 4.3% Sn sample at 125, 175, and 300 K, respectively. Similarly for the 5.2% Sn sample, [$E_D - E_{ID}$] is about 23, 20, and 29 meV at 125, 175, and 300 K, respectively. Thus, the [E_D(T) – E_{ID}(T)] values evaluated at 125 or 175 K and those evaluated at 300 K are only about 3–4 meV different for 4.3% Sn, and only about 6–9 meV different for 5.2% Sn. This difference between lower T (125 or 175 K) and 300 K is negligible compared with the possible error ranges discussed above. This fact together with about same slope of the E_D(y) fitting line for 125, 175, and 300 K strongly implies that the cross-over points shown in Figs. 3(b) and 4(b) are equally valid at room temperature as well. Therefore, based on the current analysis, we believe that the T-dependent PL presented here provides convincing evidence of the true indirect-to-direct bandgap transition for unstrained $Ge_{1-y}Sn_y$ at an Sn concentration of about 6.7%. This result is in satisfactory agreement with the result of indirect-direct crossover composition of $y = 0.073^{+0.007}_{-0.006}$ obtained in Ref. 6, given the different approaches followed in data analysis.

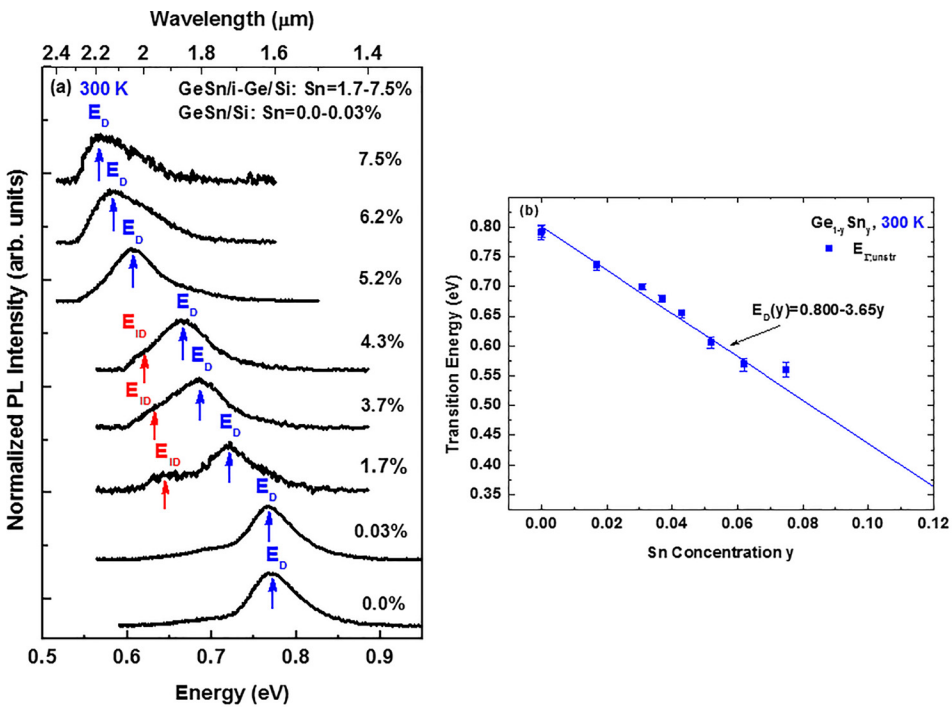

FIG. 5. (a) The PL spectra taken at room temperature for epitaxial $Ge_{1-y}Sn_y$ alloys (y = 0%–7.5%) plotted as a function of Sn content. The best estimated direct bandgap emission peak E_D (blue) and indirect bandgap emission peak E_{ID} (red) are indicated with arrows wherever possible. (b) E_D (blue squares and curve) PL peak energies at 300 K plotted as a function of Sn concentration. All these PL peak values were strain corrected for relaxed epitaxial $Ge_{1-y}Sn_y$ alloys with error bars. The fitting curve was drawn using a linear fit with a slope of 3.65 for E_D.

IV. CONCLUSION

The temperature- (T-) dependent photoluminescence (PL) spectra of various $Ge_{1-y}Sn_y$ samples ($y = 0\%–7.5\%$) were investigated at temperatures ranging from 10–300 K. The $Ge_{1-y}Sn_y$ samples grown on Si or Ge-buffered Si substrates for $Sn \leq 1.7\%$ had tensile strains (0.11%–0.19%), whereas those grown on Ge buffer layers grown on Si substrates for $Sn \geq 3.1\%$ had compressive strains (0.05%–0.13%). All these $Ge_{1-y}Sn_y$ samples show direct bandgap (E_D) PL emission and/or indirect bandgap (E_{ID}) PL emission at a given temperature. E_{ID} PL emission was generally dominant at lower temperatures (Ts) while E_D emission was dominant at higher Ts up to room temperature. At 300 K, most $Ge_{1-y}Sn_y$ samples show very weak E_{ID} emission, but exhibit one broad, dominant E_D emission peak, which could be the superposition of HH and LH transitions. However, at 10 K dominant E_D emission appears only for $Ge_{1-y}Sn_y$ with Sn content greater than 5.2%. Among other samples, T-dependent PL spectra of unintentionally doped $Ge_{0.957}Sn_{0.043}$ and $Ge_{0.948}Sn_{0.052}$ samples show clearly distinguished E_D and E_{ID} PL peaks at nearly all temperatures, which are not readily observable for other samples. Furthermore, at 125 and 175 K, both the E_D and E_{ID} PL peaks were clearly observed for most $Ge_{1-y}Sn_y$ samples. These well resolved emission peak energies of E_{ID} and E_D obtained at both 125 and 175 K were plotted as a function of Sn concentration (0%–7.5%) after correcting for strain effects, and the results show that the indirect-to-direct bandgap cross-over occurs at ~6.7% Sn for unstrained $Ge_{1-y}Sn_y$. It is believed that this true indirect-to-direct bandgap cross-over of $Ge_{1-y}Sn_y$ might also take place at about the same Sn content at room temperature. This observation suggests that the tremendous recent progress in crystal growth has finally made the development of true direct bandgap $Ge_{1-y}Sn_y$ semiconductors possible. Furthermore, these direct bandgap $Ge_{1-y}Sn_y$ alloys could become very useful for the development of next-generation optoelectronic devices, which can be fully integrated with Si technology on a single chip under CMOS compatible conditions.

ACKNOWLEDGMENTS

The authors would like to express their sincere appreciation to Dr. Gernot S. Pomrenke of the Air Force Office of Scientific Research for his support of this work. This research (MYR) was also supported in part by Basic Science Research Program through the National Research Foundation of Korea (NRF) funded by the Ministry of Education, Science and Technology (NRF-2013R1A1A2A10058310). This research (M.Y.R. and B.W.) was supported in part by an appointment to the Faculty Research Participation Program at AFIT, administered by the Oak Ridge Institute for Science and Education through an interagency agreement between the U.S. Department of Energy and AFIT.

The views expressed in this article are those of the authors and do not reflect the official policy or position of the United States Air Force, Department of Defense, or the United States Government.

[1]M. Casalino, Int. J. Opt. Appl. **2**, 1 (2012).
[2]G. T. Reed and C. E. Jason Png, Mater. Today **8**, 40 (2005).
[3]R. A. Soref, S. J. Emerlett, and W. R. Buchwald, J. Opt. A: Pure Appl. Opt. **8**, 840 (2006).
[4]S. Gupta, B. Magyari-Köpe, Y. Nishi, and K. C. Saraswat, J. Appl. Phys. **113**, 073707 (2013).
[5]J. D. Gallagher, C. L. Senaratne, J. Kouvetakis, and J. Menéndez, Appl. Phys. Lett. **105**, 142102 (2014).
[6]L. Jiang, J. D. Gallagher, C. L. Senaratne, T. Aoki, J. Mattews, J. Kouvetakis, and J. Menéndez, Semicond. Sci. Technol. **29**, 115028 (2014).
[7]S. A. Ghetmiri, W. Du, B. R. Conley, A. Mosleh, A. Nazzal, G. Sun, R. A. Soref, J. Margetis, J. Tolle, H. A. Naseem, and S.-Q. Yu, J. Vac. Sci. Technol. B **32**, 060601 (2014).
[8]S. Wirths, R. Geiger, N. von den Driesch, G. Mussler, T. Stoica, S. Manti, Z. Ikonic, M. Luysberg, S. Chiussi, J. M. Hartmann, H. Sigg, J. Faist, D. Buca, and D. Grützmacher, Nat. Photonics **9**, 88 (2015).
[9]V. Chakraborty, B. Mukhapadhyay, and P. K. Basu, Physica E **50**, 67 (2013).
[10]W. Du, Y. Zhou, S. A. Ghetmiri, A. Mosleh, B. R. Conley, A. Nazzal, R. A. Soref, G. Sun, J. Tolle, J. Margetis, H. A. Naseem, and S.-Q. Yu, Appl. Phys. Lett. **104**, 241110 (2014).
[11]R. Roucka, J. Mathews, R. T. Beeler, J. Tolle, J. Kouvetakis, and J. Menéndez, Appl. Phys. Lett. **98**, 061109 (2011).
[12]R. Roucka, R. Beeler, J. Mathews, M.-Y. Ryu, Y. K. Yeo, J. Menéndez, and J. Kouvetakis, J. Appl. Phys. **109**, 103115 (2011).
[13]M. Oehme, M. Schmid, M. Kaschel, M. Gollhofer, D. Widmann, E. Kasper, and J. Schulze, Appl. Phys. Lett. **101**, 141110 (2012).
[14]K. P. Homewood and M. A. Lourenco, Nat. Photonics **9**, 78 (2015).
[15]M.-Y. Ryu, T. R. Harris, Y. K. Yeo, R. T. Beeler, and J. Kouvetakis, Appl. Phys. Lett. **102**, 171908 (2013).
[16]T. R. Harris, Y. K. Yeo, M.-Y. Ryu, R. T. Beeler, and J. Kouvekakis, J. Appl. Phys. **116**, 103502 (2014).
[17]H.-J. Jo, M. G. So, J. S. Kim, M.-Y. Ryu, Y. K. Yeo, and J. Kouvetakis, Thin Solid Films **591**, 295 (2015).
[18]D. Stange, S. Wirths, N. von den Driesch, G. Mussler, T. Stoica, Z. Ikonic, J. M. Hartmann, S. Mantl, D. Grützmacher, and D. Buca, ACS Photonics **2**, 1539 (2015).
[19]S. Al-Kabi, S. A. Ghertmiri, J. Margetis, W. Du, A. Mosleh, M. Alher, W. Dou, J. M. Grant, G. Sun, R. A. Soref, J. Tolle, B. Li, M. Mortazavi, H. A. Naseem, and S.-Q. Yu, J. Electron. Mater. **45**, 2133 (2016).
[20]C. L. Senaratne, J. D. Gallagher, L. Jiang, T. Aoki, D. J. Smith, J. Menéndez, and J. Kouvetakis, J. Appl. Phys. **116**, 133509 (2014).
[21]J. R. Haynes, M. Lax, and W. F. Flood, J. Phys. Chem. Solids **8**, 392 (1959).
[22]Y. P. Varshni, Physica **34**, 149 (1967).
[23]M. E. Levinshten, S. L. Rumyantsev, and M. Shur, *Handbook Series on Semiconductor Parameters, Volume 1: Si, Ge, C (Diamond), GaAs,GaP, GaSb, InAs, InP, InSb* (World Scientific, London, 1996).
[24]C. G. Van de Walle, Phys. Rev. B **39**, 1871 (1989).